

ON THE ACCURACY OF THE NUMERICAL DETECTION OF COMPLEX OBSTACLES FROM FAR FIELD DATA USING THE PROBE METHOD*

J. J. LIU[†] AND M. SINI[‡]

Abstract. We deal with the acoustic inverse scattering problem for detecting an obstacle with mixed boundary conditions from the far field map. We show how the geometrical properties and the material parameter distributed on the surface are involved in the obstacle reconstruction numerically. The main advance of this research is the numerical analysis and implementation of our recent theoretical work [J.J. Liu and M. Sini, *How to make the reconstruction of obstacles more (or less) accurate from exterior measurements*, RICAM preprint 2008-04, Johann Radon Institute for Computational and Applied Mathematics, Linz, Austria, 2008] regarding the higher order asymptotic expansion of the probe indicator function and the introduction of complex-valued surface impedance. An efficient numerical implementation scheme is proposed based on the properties of minimum norm solutions. Precisely, using the relation between the surface impedance and the obstacle curvature contained in the higher order expansion of the indicators, we reveal how the obstacle curvature and the surface impedance on the coated part influence the blowing-up behavior. Using this theoretical result, we can specify the complex surface impedance in terms of the obstacle curvature to make the reconstruction more (or less) accurate. By establishing properties of the minimum norm solution for approximating the singular sources, efficient realizations for approximating the multipoles by the Herglotz wave function and therefore the implementations of the probe methods are developed with an error estimate. We finally show extensive numerical tests explaining how and to what extent the coupling relation between the curvature and the surface impedance changes the accuracy of the reconstruction of the obstacles.

Key words. inverse scattering, far field, impedance boundary, regularization, minimum norm solution, numerics

AMS subject classifications. 35P25, 35R30, 45Q05, 78A45

DOI. 10.1137/080718024

1. Introduction. The inverse scattering problems by complex impenetrable obstacles have received much attention in recent years due to their potential applications; see, for instance, [3, 8, 24] for different analytical methods and [2, 12] for practical motivations in military coatings and marine acoustics. By a complex obstacle, we mean an obstacle whose boundary is characterized by its geometry as well as the acoustic properties modeled by appropriate material distributed along a part or the whole surface. In this paper, our inversion input data are far field patterns produced by many incident plane waves, with the goal of reconstructing the complex obstacle from these data. Instead of considering a full 3-dimensional electromagnetism model, we restrict ourselves to the 2-dimensional Helmholtz model. This latter model is deduced from the former one in case the obstacle is a cylinder and the incident field is appropriately polarized; see [3].

This problem has quite a long history; see, for instance, [6, 4, 3, 5, 8, 14, 10, 22, 23, 24]. There are several methods proposed to solve this problem. We are interested

*Received by the editors March 10, 2008; accepted for publication (in revised form) March 6, 2009; published electronically June 25, 2009.

<http://www.siam.org/journals/sisc/31-4/71802.html>

[†]Department of Mathematics, Southeast University, Nanjing, 210096, People's Republic of China (jjliu@seu.edu.cn). The work of this author was supported by NSFC(10771033).

[‡]Johann Radon Institute for Computational and Applied Mathematics, Austrian Academy of Science, Linz, A-4040, Austria (mourad.sini@oeaw.ac.at). The work of this author was supported by FWF of the Austrian Academy of Sciences through the project SFB F1308.

in the noniterative ones, such as the linear sampling method [7], the factorization method [15], the multiple signal classification (MUSIC) algorithm [1, 9], the probe method [13], and the singular sources method [21]. All these methods build indicator functions depending on a parameter given by the source points. The reconstruction of the shape of the obstacle, by these methods, is based on the drastic behavior of the corresponding indicator functions when the source point approaches the interface of the obstacle. In our opinion, the way that these indicator functions blowup is the crucial point in order to understand the numerical performance of these theoretically elegant reconstruction methods.

In a recent work [17, 19], we started such studies by taking as pilot the probing method (as the probe and the singular sources methods, see [11, 20]). Precisely, using multipoles of order two as point sources, we derived in [17] the asymptotic expansion of the indicator functions with respect to the source point. We found out that the first order term in the expansion involves the unit normals of the interface, while the second (lower) order term involves a combination of the surface curvature and the imaginary part of the surface impedance. This behavior may explain why, for example, reconstructing convex objects is easier and more accurate than reconstructing nonconvex ones. In addition, this analysis also suggests some possible ways for making the reconstruction more (or less) accurate by using the artificially introduced *complex* surface impedance. We think that these new observations may have some potential applications, for instance, in military coatings, see [12], and marine acoustics, see [2].

Let D be a bounded domain of \mathbb{R}^2 with its boundary $\partial D \in C^{2,1}$, and $\mathbb{R}^2 \setminus \overline{D}$ is connected. We assume that ∂D has the decomposition $\partial D = \overline{\partial D_I} \cup \overline{\partial D_D}$, $\partial D_I \cap \partial D_D = \emptyset$, where ∂D_D and ∂D_I are open curves in ∂D .

For given incident plane wave $u^i(x) = e^{ikd \cdot x}$, we associate the total wave $u(x) = u^i(x) + u^s(x)$ satisfying the following exterior problem

$$(1.1) \quad \begin{cases} \Delta u + \kappa^2 u = 0 & \text{in } \mathbb{R}^2 \setminus \overline{D}, \\ u = 0 & \text{on } \partial D_D, \\ \frac{\partial u}{\partial \nu} + i\kappa\sigma u = 0 & \text{on } \partial D_I, \end{cases}$$

where the scattered fields u^s satisfy the Sommerfeld radiation condition

$$(1.2) \quad \lim_{|x| \rightarrow \infty} \sqrt{|x|} \left(\frac{\partial u^s}{\partial |x|} - i\kappa u^s \right) = 0,$$

with $\nu(x)$ as the outward normal direction of ∂D . We assume that the surface impedance $\sigma(x) := \sigma^r(x) + i\sigma^i(x)$ is a complex-valued Lipschitz continuous function, and its real part $\sigma^r(x)$ has a uniform lower bound $\sigma_0^r > 0$ on ∂D_I . The part ∂D_I is referred to by the coated part of ∂D , and ∂D_D is the noncoated part.

The mixed problem (1.1)–(1.2) is well posed. More generally, for $g \in H^{\frac{1}{2}}(\partial D_D)$ and $h \in H^{-\frac{1}{2}}(\partial D_I)$, there exists a unique solution of the mixed problem

$$(1.3) \quad \begin{cases} \Delta u + \kappa^2 u = 0 & \text{in } \mathbb{R}^2 \setminus \overline{D}, \\ u = g & \text{on } \partial D_D, \\ \frac{\partial u}{\partial \nu} + i\kappa\sigma u = h & \text{on } \partial D_I, \\ \frac{\partial u}{\partial r} - i\kappa u = o\left(\frac{1}{\sqrt{r}}\right), & r \rightarrow \infty, \end{cases}$$

and the solution satisfies

$$(1.4) \quad \|u\|_{H^1(\Omega_R \cap (\mathbb{R}^2 \setminus \overline{D}))} \leq C_R (\|g\|_{H^{1/2}(\partial D_D)} + \|h\|_{H^{-1/2}(\partial D_I)}),$$

where Ω_R is a disk of radius R and C_R is positive constant; see [3] for more details.

It is also well-known that the scattered field u^s has the asymptotic expansion

$$(1.5) \quad u^s(x, d) = \frac{e^{i\kappa|x|}}{\sqrt{|x|}} \left(u^\infty(\hat{x}, d) + O\left(\frac{1}{|x|}\right) \right), \quad \hat{x} = \frac{x}{|x|} \in \mathbb{S},$$

as $|x| \rightarrow \infty$, where \mathbb{S} is the unit cycle in \mathbb{R}^2 . $u^\infty(\hat{x}, d)$ is called the far field pattern of the scattered wave $u^s(x, d)$.

For the above scattering problem by a complex obstacle, the inverse scattering problem is stated as follows.

Given $u^\infty(\cdot, \cdot)$ on $\mathbb{S} \times \mathbb{S}$ for the scattering problem (1.1)–(1.2), we need to

- reconstruct the shape of the obstacle D ;
- reconstruct some geometrical properties of ∂D such as normal directions and the curvature;
- distinguish the coated part ∂D_I from the noncoated part ∂D_D ;
- reconstruct the complex surface impedance $\sigma(x)$ on ∂D_I , including the real and the imaginary parts.

Remark 1.1. Theoretically speaking, both the normal direction of ∂D and the curvature are completely determined once ∂D is known. However, since ∂D is reconstructed approximately in the inverse scattering problem, the determination of the obstacle curvature and the normal directions from the approximate ∂D is ill-posed. From the numerical point of view, we need to detect these two pieces of geometric information from the far field data directly.

The aim of this paper is to propose an efficient realization of the probe method using the higher order expansions of its indicator function as proposed in [17] and to analyze the reconstruction accuracy mathematically. Although from the theoretical asymptotic expansions we can reconstruct both the boundary shape and boundary impedance for the complex obstacle, in this paper we focus on the issue of how the specified surface impedance influences the shape reconstruction accuracy. This is an important new ingredient revealed from the higher order expansion of indicators. More precisely, we address the following three points in this paper:

- How to construct the indicator functions numerically and efficiently.
- Numerical implementations to show reconstructions of complex obstacles.
Since the probe method (and actually any of the previously mentioned probing or sampling methods) uses the limit behavior of some indicator functions to probe the obstacle boundary as well as the surface impedance, the numerical performance of this theoretically elegant method is of great importance for its practical application. That is, we need to understand to what extent this method can approximate the unknown ingredients numerically and what is the amount of computation. In addition and in particular, the probe method uses some needle to detect the boundary points from all the directions. Therefore we need its efficient realization.
- Numerical implementations to show how we can increase or decrease the accuracy of the shape reconstruction of an obstacle by balancing the surface impedance and the obstacle curvature.

As we already mentioned, in our previous paper [17] we showed that the combined effect of the surface impedance and the concavity of the obstacle makes the scattering

process much more complicated. However, by using explicit combinations of the surface impedance and the curvature, we show that the accuracy of reconstructing the obstacle can be controlled. The key idea is to change the blowing-up behavior of the indicator functions by adjusting the relation between surface impedance and the obstacle curvature. To the best of our knowledge, the research of inverse scattering problems up to now always considered the case $\sigma^i(x) = 0$. We will see that the introduction of a nonzero $\sigma^i(x)$ has a big numerical influence on the shape reconstruction of an obstacle.

We would like to emphasize that, although the notion of accuracy is normally method-dependent, we believe that, regarding the interface reconstruction, what we are saying is independent of the method used and it is inherent to the problem itself. This is due to the fact that we are basically using the whole Green's function of the forward problem to state the reconstruction methods, and we know that Green's functions characterize completely the problem.

This paper is organized as follows. In section 2, we state the asymptotic expansion results presented in [17] and rewrite them in an equivalent way. Such an equivalent form is important for our numerical realizations. Then in section 3, we discuss the efficient approximation of the multipoles on the boundary of the approximate domains by establishing the properties of minimum norm solutions. The error estimate on the singular source approximation as well as the choice of the dimension of the approximate function spaces, which has an important role in the construction of the indicator function, are given in section 4. Finally, we present some numerical results in section 5 by the proposed realization schemes, supporting our theoretical analysis.

2. Presentation of the asymptotic results and equivalent forms. Due to the superposition principle, the scattered field associated with the Herglotz incident field $v_g^i := v_g(x)$ defined by

$$(2.1) \quad v_g(x) := \int_{\mathbb{S}} e^{i\kappa x \cdot d} g(d) \, ds(d), \quad x \in \mathbb{R}^2,$$

with $g \in L^2(\mathbb{S})$ is given by

$$(2.2) \quad v_g^s(x) := \int_{\mathbb{S}} u^s(x, d) g(d) \, ds(d), \quad x \in \mathbb{R}^2 \setminus \overline{D},$$

and its far field is

$$(2.3) \quad v_g^\infty(\hat{x}) := \int_{S^1} u^\infty(\hat{x}, d) g(d) \, ds(d), \quad \hat{x} \in \mathbb{S}.$$

Denote by $\Phi(x, z) = \frac{i}{4} H_0^{(1)}(\kappa|x-z|)$ the fundamental solution for the Helmholtz equation in \mathbb{R}^2 . Assume that $\overline{D} \subset \subset \Omega$ for some known Ω with smooth boundary. For $a \in \Omega \setminus D$, denote by $\{z_p\} \subset \Omega \setminus \overline{D}$ a sequence tending to a and starting from $\partial\Omega$. For any z_p , set D_a^p to be a C^2 -regular domain such that $\overline{D} \subset D_a^p$ and $\partial\overline{D} \subset D_a^p$ with $z_q \in \Omega \setminus \overline{D_a^p}$ for every $q = 1, 2, \dots, p$ and that the Dirichlet interior problem on D_a^p for the Helmholtz equation is uniquely solvable. In this case, the Herglotz wave operator \mathbb{H} from $L^2(\mathbb{S})$ to $L^2(\partial D_a^p)$ defined by

$$(2.4) \quad \mathbb{H}[g](x) := v_g(x) = \int_{\mathbb{S}} e^{i\kappa x \cdot d} g(d) \, ds(d)$$

is injective, compact with dense range; see [8]. Now we consider the sequence of point sources: pole $\Phi(\cdot, z_p)$, dipoles $\frac{\partial}{\partial x_j} \Phi(\cdot, z)$, and multipoles of order two $\frac{\partial}{\partial x_j} \frac{\partial}{\partial x_2} \Phi(\cdot, z)$

for $j = 1, 2$. For every p fixed, we construct three density sequences $\{g_n^p\}$, $\{f_m^{j,p}\}$, and $\{h_k^{j,p}\}$ in $L^2(\mathbb{S})$ with $j = 1, 2$ by the Tikhonov regularization such that

$$(2.5) \quad \|v_{g_n^p} - \Phi(\cdot, z_p)\|_{L^2(\partial D_a^p)} \rightarrow 0, \quad n \rightarrow \infty,$$

$$(2.6) \quad \left\| v_{f_m^{j,p}} - \frac{\partial}{\partial x_j} \Phi(\cdot, z_p) \right\|_{L^2(\partial D_a^p)} \rightarrow 0, \quad m \rightarrow \infty,$$

$$(2.7) \quad \left\| v_{h_k^{j,p}} - \frac{\partial}{\partial x_j} \frac{\partial}{\partial x_2} \Phi(\cdot, z_p) \right\|_{L^2(\partial D_a^p)} \rightarrow 0, \quad k \rightarrow \infty.$$

Using these three density sequences, we construct the following three indicators:

$$(2.8) \quad I^0(z_p) := \frac{1}{\gamma_2} \lim_{m \rightarrow \infty} \lim_{n \rightarrow \infty} \int_{\mathbb{S}} \int_{\mathbb{S}} u^\infty(-\hat{x}, d) g_m^p(d) g_n^p(\hat{x}) ds(\hat{x}) ds(d),$$

$$(2.9) \quad I_j^1(z_p) := \frac{1}{\gamma_2} \lim_{m \rightarrow \infty} \lim_{n \rightarrow \infty} \int_{\mathbb{S}} \int_{\mathbb{S}} u^\infty(-\hat{x}, d) f_m^{j,p}(d) g_n^p(\hat{x}) ds(\hat{x}) ds(d),$$

$$(2.10) \quad I_j^2(z_p) := \frac{1}{\gamma_2} \lim_{m \rightarrow \infty} \lim_{n \rightarrow \infty} \int_{\mathbb{S}} \int_{\mathbb{S}} u^\infty(-\hat{x}, d) h_m^{j,p}(d) g_n^p(\hat{x}) ds(\hat{x}) ds(d),$$

where $\gamma_2 = e^{i\pi/4} / \sqrt{8\pi\kappa}$.

For the points $a \in \partial D$, we choose the sequence $\{z_p\}_{p \in \mathbb{N}}$ included in $C_{a,\theta}$, where $C_{a,\theta}$ is a cone with center a , angle $\theta \in [0, \frac{\pi}{2})$, and axis $\nu(a)$. Denote by $\mathcal{C}(a)$ the curvature of ∂D at point a . The following theoretical result is given in [17].

THEOREM 2.1. *Assume that the boundary ∂D is of class $C^{2,1}$ and $\sigma = \sigma^r + i\sigma^i$ defined on ∂D_I is a complex-valued Lipschitz function with positive real part. Then the above three indicators have the following asymptotic formulas:*

I. For pole $\Phi(x, z)$ as source, it follows that

$$(2.11) \quad \operatorname{Re} I^0(z_p) = \begin{cases} -\frac{1}{4\pi} \ln |(z_p - a) \cdot \nu(a)| + O(1), & a \in \partial D_I, \\ +\frac{1}{4\pi} \ln |(z_p - a) \cdot \nu(a)| + O(1), & a \in \partial D_D, \end{cases}$$

$$(2.12) \quad \operatorname{Im} I^0(z_p) = O(1), \quad a \in \partial D.$$

II. Using dipoles $\frac{\partial}{\partial x_j} \Phi(x, z)$ with $j = 1, 2$ as sources, it follows that

$$(2.13) \quad \operatorname{Re} I_j^1(z_p) = \begin{cases} \frac{-\nu_j(a)}{4\pi |(z_p - a) \cdot \nu(a)|} - \frac{\nu_j(a)(\kappa\sigma^i(a) + \frac{1}{2}\mathcal{C}(a))}{\pi} \ln |(z_p - a) \cdot \nu(a)| + O(1), & a \in \partial D_I, \\ \frac{\nu_j(a)}{4\pi |(z_p - a) \cdot \nu(a)|} - \frac{\nu_j(a)\mathcal{C}(a)}{2\pi} \ln |(z_p - a) \cdot \nu(a)| + O(1), & a \in \partial D_D, \end{cases}$$

$$(2.14) \quad \operatorname{Im} I_j^1(z_p) = \begin{cases} -\frac{\nu_j(a)\kappa\sigma^r(a)}{\pi} \ln |(z_p - a) \cdot \nu(a)| + O(1), & a \in \partial D_I, \\ O(1), & a \in \partial D_D. \end{cases}$$

III. Using multipoles of order two $\frac{\partial}{\partial x_j} \frac{\partial}{\partial x_2} \Phi(x, z)$ with $j = 1, 2$, it follows that

$$(2.15) \quad \operatorname{Re} I_1^2(z_p) = \begin{cases} \frac{\nu_1(a)\nu_2(a)}{4\pi |(z_p - a) \cdot \nu(a)|^2} - \frac{\nu_1(a)\nu_2(a)}{\pi} \left[\kappa\sigma^i(a) + \frac{3}{4}\mathcal{C}(a) \right] \frac{1}{|(z_p - a) \cdot \nu(a)|} \\ \quad + O(\ln |(z_p - a) \cdot \nu(a)|), & a \in \partial D_I, \\ \frac{-\nu_1(a)\nu_2(a)}{4\pi |(z_p - a) \cdot \nu(a)|^2} - \frac{3\nu_1(a)\nu_2(a)}{4\pi} \mathcal{C}(a) \frac{1}{|(z_p - a) \cdot \nu(a)|} \\ \quad + O(\ln |(z_p - a) \cdot \nu(a)|), & a \in \partial D_D, \end{cases}$$

(2.16)

$$\operatorname{Re} I_2^2(z_p) = \begin{cases} \frac{\nu_2^2(a) - \nu_1^2(a)}{8\pi|(z_p - a) \cdot \nu(a)|^2} - \frac{\nu_2^2(a) - \nu_1^2(a)}{2\pi} \left[\kappa\sigma^i(a) + \frac{3}{4}\mathcal{C}(a) \right] \frac{1}{|(z_p - a) \cdot \nu(a)|} \\ \quad + O(\ln |(z_p - a) \cdot \nu(a)|), & a \in \partial D_I, \\ \frac{\nu_1^2(a) - \nu_2^2(a)}{8\pi|(z_p - a) \cdot \nu(a)|^2} - \frac{3(\nu_2^2(a) - \nu_1^2(a))}{8\pi} \mathcal{C}(a) \frac{1}{|(z_p - a) \cdot \nu(a)|} \\ \quad + O(\ln |(z_p - a) \cdot \nu(a)|), & a \in \partial D_D, \end{cases}$$

and

$$(2.17) \quad \operatorname{Im} I_1^2(z_p) = \begin{cases} \frac{\nu_1(a)\nu_2(a)}{\pi|(z_p - a) \cdot \nu(a)|} \kappa\sigma^r + O(\ln |(z_p - a) \cdot \nu(a)|), & a \in \partial D_I, \\ O(\ln |(z_p - a) \cdot \nu(a)|), & a \in \partial D_D, \end{cases}$$

$$(2.18) \quad \operatorname{Im} I_2^2(z_p) = \begin{cases} \frac{\nu_2^2(a) - \nu_1^2(a)}{2\pi|(z_p - a) \cdot \nu(a)|} \kappa\sigma^r + O(\ln |(z_p - a) \cdot \nu(a)|), & a \in \partial D_I, \\ O(\ln |(z_p - a) \cdot \nu(a)|), & a \in \partial D_D. \end{cases}$$

The above theoretical results will be used in our numerical realizations in different but equivalent forms for reconstructing the obstacle. These formulas can be used in the following situations.

1. The obstacles are unknown. In this case, we know nothing about the obstacle shape, boundary type, and surface impedance. However, the combination of the above formulas enables us to detect the obstacle without the knowledge of surface impedance.

- Use (2.11) to detect the boundary shape and the type, that is,

$$(2.19) \quad \lim_{z_p \rightarrow a} \operatorname{Re} I^0(z_p) = \begin{cases} +\infty, & a \in \partial D_I, \\ -\infty, & a \in \partial D_D. \end{cases}$$

The other way to detect the location and type of ∂D is

(2.20)

$$\lim_{z_p \rightarrow a} \sum_{j=1}^2 (\operatorname{Re} I_j^1)^2 = \begin{cases} \lim_{z_p \rightarrow a} \left[\frac{1}{16\pi^2|(z_p - a) \cdot \nu(a)|^2} - \frac{(\kappa\sigma^i + \frac{1}{2}\mathcal{C}(a)) \ln |(z_p - a) \cdot \nu(a)|}{2\pi^2|(z_p - a) \cdot \nu(a)|} \right] \\ \quad + O\left(\frac{1}{4\pi|(z_p - a) \cdot \nu(a)|}\right) = +\infty, & a \in \partial D_I, \\ \lim_{z_p \rightarrow a} \left[\frac{1}{16\pi^2|(z_p - a) \cdot \nu(a)|^2} - \frac{\mathcal{C}(a) \ln |(z_p - a) \cdot \nu(a)|}{8\pi^2|(z_p - a) \cdot \nu(a)|} \right] \\ \quad + O\left(\frac{1}{4\pi|(z_p - a) \cdot \nu(a)|}\right) = +\infty, & a \in \partial D_D, \end{cases}$$

$$(2.21) \quad \lim_{z_p \rightarrow a} \sum_{j=1}^2 (\operatorname{Im} I_j^1)^2 = \begin{cases} \frac{(\kappa\sigma^r)^2}{\pi^2} \lim_{z_p \rightarrow a} \ln^2 |(z_p - a) \cdot \nu(a)| \\ \quad + O(\ln |(z_p - a) \cdot \nu(a)|) = +\infty, & a \in \partial D_I, \\ O(1), & a \in \partial D_D, \end{cases}$$

in terms of (2.13) and (2.14). We can also use the corresponding formulas for $\text{Re } I_j^2$ and $\text{Im } I_j^2$ for $j = 1, 2$. Then the boundary points can be approximated by solving one of the following level curve equations:

$$(2.22) \quad |\text{Re} I^0(z)| = C, \quad |(\text{Re} I_1^1(z), \text{Re} I_2^1(z))| = C, \quad \text{or} \quad |(\text{Re} I_1^2(z), \text{Re} I_2^2(z))| = C,$$

where C is some constant taken to be large. By analyzing the previous asymptotic behaviors, it is suggested to use (2.20) for detecting the shape and to use (2.19) for detecting the type.

- The above formula can give only an approximation to ∂D numerically. Therefore the normal vector $\nu(a)$ may be of large error using the approximation of ∂D obtained from (2.19) or (2.20). However, using the dipoles formulas (2.13), the normal direction can be determined as

$$(2.23) \quad \nu(a) = \left(\pm t \sqrt{\frac{1}{1+t^2}}, \pm \sqrt{\frac{1}{1+t^2}} \right), \quad \text{where } t := \lim_{z_p \rightarrow a} \frac{\text{Re } I_1^1(z_p)}{\text{Re } I_2^1(z_p)} = \frac{\nu_1(a)}{\nu_2(a)}$$

almost everywhere, except for some points satisfying $\nu_2(a) = 0$. In the case that t is quite large, which means $\nu_2(a) \approx 0$, the normal direction at a can be computed from

$$(2.24) \quad \nu(a) = \left(\pm \sqrt{\frac{1}{1+\tilde{t}^2}}, \pm \tilde{t} \sqrt{\frac{1}{1+\tilde{t}^2}} \right), \quad \text{where } \tilde{t} := \lim_{z_p \rightarrow a} \frac{\text{Re } I_2^1(z_p)}{\text{Re } I_1^1(z_p)} = \frac{\nu_2(a)}{\nu_1(a)}.$$

The sign \pm can be fixed by the orientation of ∂D and the rough reconstruction of ∂D . More precisely, for $\nu = (x'_2(t), -x'_1(t))$, the sign of each component can be determined from the tangential direction $\tau := (x'_1(t), x'_2(t))$ of a reasonable approximation of ∂D . That is, a reasonable approximation of ∂D can give us the correct sign of each component of τ .

- Using the multipoles formulas, the curvature and the imaginary part of the surface impedance σ^i can be computed from the known (or already computed) normal direction of ∂D . If the point a is on ∂D_I , then we start to compute the two quantities

$$(2.25) \quad \frac{3}{4} \mathcal{C}(a) + \kappa \sigma^i(a) = -2 \lim_{z_p \rightarrow a} \left[\frac{\pi((2\nu_1(a)\nu_2(a)\text{Re} I_1^2(z_p) + (\nu_2^2(a) - \nu_1^2(a))\text{Re} I_2^2(z_p)))}{|(z_p - a) \cdot \nu(a)|^{-1}} - \frac{1}{8|(z_p - a) \cdot \nu(a)|} \right],$$

$$(2.26) \quad \frac{1}{2} \mathcal{C}(a) + \kappa \sigma^i(a) = - \lim_{z_p \rightarrow a} \frac{\pi \sum_{j=1}^2 \nu_j(a) \text{Re} I_j^1(z_p) + \frac{1}{4|(z_p - a) \cdot \nu(a)|}}{\ln |(z_p - a) \cdot \nu(a)|}$$

from which we deduce the values of $\mathcal{C}(a)$ and $\sigma^i(a)$.

If a is on ∂D_D , then we have either

$$\mathcal{C}(a) = -\frac{8}{3} \lim_{z_p \rightarrow a} \left[\frac{\pi(2\nu_1(a)\nu_2(a)\text{Re} I_1^2(z_p) + (\nu_2^2(a) - \nu_1^2(a))\text{Re} I_2^2(z_p))}{|(z_p - a) \cdot \nu(a)|^{-1}} + \frac{1}{8|(z_p - a) \cdot \nu(a)|} \right]$$

using multipoles of order two as sources or

$$\mathcal{C}(a) = -2 \lim_{z_p \rightarrow a} \frac{\pi \sum_{j=1}^2 \nu_j(a) \operatorname{Re} I_j^1(z_p) - \frac{1}{4|(z_p-a) \cdot \nu(a)|}}{\ln |(z_p - a) \cdot \nu(a)|}$$

using multipoles of first order as sources.

- The geometrical properties of the obstacle, the type of boundary conditions, and the imaginary part of the surface impedance have been determined by the above two steps; now we can determine the real part of the surface impedance by (2.13). That is,

$$(2.27) \quad \sigma^r(a) = - \lim_{z_p \rightarrow a} \frac{\pi \sum_{j=1}^2 \nu_j(a) \operatorname{Im} I_j^1(z_p)}{\kappa \ln |(z_p - a) \cdot \nu(a)|}, \quad a \in D_I.$$

Using (2.17) and (2.18), we can identify $\sigma^r(x)$ from the other formula:

$$\frac{2\pi}{\kappa} \lim_{z_p \rightarrow a} \frac{2\nu_1(a)\nu_2(a)\operatorname{Im} I_1^2(z_p) + (\nu_2^2(a) - \nu_1^2(a))\operatorname{Im} I_2^2(z_p)}{|(z_p - a) \cdot \nu(a)|^{-1}} = \sigma^r(a), a \in \partial D_I.$$

2. The obstacles are known. Even though the first term in the asymptotic of all the indicator functions is the dominant term, in numerically solving the level curve equations (2.22), the lower order terms play a key role. So, we need to take them into account in interpreting the accuracy of the computed shape. Hence by controlling these terms, we can control the accuracy of the reconstruction. Here we explain how adjusting the relation between the curvature and the surface impedance can improve or destroy the accuracy of the reconstruction.

- If we know the obstacle shape and wish to make it detectable with more accuracy, then we can choose the surface impedance (the coating coefficient) distributed in terms of the curvature in some suitable way. More precisely, the asymptotic behaviors

$$(2.28) \quad \sum_{j=1}^2 (\operatorname{Re} R_j^1)^2 = \frac{1}{16\pi^2 |(z_p - a) \cdot \nu(a)|^2} - \frac{(\kappa\sigma^i + \frac{1}{2}\mathcal{C}(a)) \ln |(z_p - a) \cdot \nu(a)|}{2\pi^2 |(z_p - a) \cdot \nu(a)|} + O\left(\frac{1}{4\pi |(z_p - a) \cdot \nu(a)|}\right)$$

for dipoles and

$$(2.29) \quad \begin{aligned} & 2\nu_1(a)\nu_2(a)\operatorname{Re} I_1^2(z_p) + (\nu_2^2(a) - \nu_1^2(a))\operatorname{Re} I_2^2(z_p) \\ &= \frac{1}{8\pi |(z_p - a) \cdot \nu(a)|^2} - \frac{\frac{3}{4}\mathcal{C}(a) + \kappa\sigma^i(a)}{\pi |(z_p - a) \cdot \nu(a)|} + O(\ln |(z_p - a) \cdot \nu(a)|) \end{aligned}$$

for multipoles provide a possible way. In fact, if we take $\partial D = \partial D_I$, i.e., distribute the coating coefficient along all the surface of the obstacle, then the uniform behavior of functions $\kappa\sigma^i(a) + \frac{1}{2}\mathcal{C}(a)$ and $\kappa\sigma^i(a) + \frac{3}{4}\mathcal{C}(a)$ on ∂D make the geometric shape ∂D easier to be detected. In this case, the blowup of the indicator functions $I_j(z)$ is, to some extent, uniform around the obstacle which makes the reconstruction of the obstacle less affected by the lower order terms. Notice that, although the signs of $\kappa\sigma^i + \frac{1}{2}\mathcal{C}(a)$ and $\kappa\sigma^i + \frac{3}{4}\mathcal{C}(a)$ in ∂D can change the value of the indicators, such an influence is not that important and the uniform feature of $\frac{1}{2}\mathcal{C}(a) + \kappa\sigma^i(a)$ is the most important.

- If we wish for the obstacle to be detectable with less accuracy, then we can choose σ^i on ∂D_I to be nonuniformly distributed (i.e., highly oscillating) so that the blowup of the indicator functions is less uniform around the obstacle. This is true for any of the indicator functions we use, i.e., $I^0(z)$ or $I_j^i(z)$ for $i, j = 1, 2$.

Notice that in our previous paper [18] for the mixed boundary condition we always assume that $\sigma^i \equiv 0$. We have seen in this paper that the introduction of nonzero σ^i has an important effect on the reconstruction of the boundary shape.

3. Construction of density function for the indicator. In this section, we consider how to compute the approximations of the point sources in ∂D_a^p efficiently, since, in detecting the obstacle boundary, the approximated domain ∂D_a^p needs to be chosen for z_p approaching ∂D along all directions. If we get this approximation always by solving the minimum norm solution in ∂D_a^p , then the amount of computation will be quite large. Notice that one key point in the detection by the probe method is to find density functions g, f , and h , such that the approximations (2.5)–(2.7) hold. Constructing these three functions by minimum norm solutions is just one possible way but not the only way.

We will show in this section that if the approximation domain D_a^p is constructed from some fixed reference domain D_0 by rotation and translation, then these three functions can be constructed from the related minimum norm solutions defined in the fixed domain ∂D_0 , using a simple function transform depending on the rotation matrix and translation vector. By this technique, the amount of computation for constructing the indicator function will be decreased dramatically.

For given fixed reference domain G_0 with $0 \notin G_0$ and smooth boundary ∂G_0 , let G be a domain generated from G_0 by rotation and translation. We assume that

$$G = \mathbb{M}G_0 + z_0,$$

with an orthogonal unit matrix \mathbb{M} and the translation vector z_0 .

Consider two integral equations of the first kind:

$$(3.1) \quad \mathbb{H}[g_0](x) = \Phi(x, 0), \quad x \in \partial G_0,$$

and

$$(3.2) \quad \mathbb{H}[g](x) = \Phi(x, z_0), \quad x \in \partial G.$$

It has been proven [21] that the following lemma holds.

LEMMA 3.1. *Assume that $g_0(d)$ is the minimum norm solution of (3.1) with discrepancy $\epsilon > 0$. Then $g(d)$ defined by*

$$(3.3) \quad g(d) = g_0(\mathbb{M}^{-1}d)e^{-i\kappa d \cdot z_0}$$

is the minimum norm solution of (3.2) with discrepancy $\epsilon > 0$.

This result means that we can determine the density function $g(d)$ using the minimum norm solution in the fixed domain G_0 from (3.3) such that

$$(3.4) \quad \|\mathbb{H}[g](\cdot) - \Phi(\cdot, z_0)\|_{L^2(\partial G)}^2 \leq \epsilon^2.$$

Next, we need to generalize this result to the cases where Φ is replaced by its partial derivatives.

For vector-valued function $(\varphi_1, \varphi_2)^T \in L^2(\mathbb{S}) \times L^2(\mathbb{S}) := L^2(\mathbb{S} \times \mathbb{S})$, define

$$\mathbb{H}[(\varphi_1, \varphi_2)^T](x) := (\mathbb{H}[\varphi_1](x), \mathbb{H}[\varphi_2](x))^T.$$

For functions $(f_1, f_2)^T \in L^2(\Gamma) \times L^2(\Gamma) := L^2(\Gamma \times \Gamma)$, we define the norm

$$\|(f_1, f_2)^T\|_{L^2(\Gamma \times \Gamma)}^2 := \|f_1\|_{L^2(\Gamma)}^2 + \|f_2\|_{L^2(\Gamma)}^2,$$

where Γ may be $\mathbb{S}, \partial G_0$, or ∂G .

THEOREM 3.2. *Assume that $f_0^j(d)$ with $j = 1, 2$ are minimum norm solutions of*

$$(3.5) \quad \mathbb{H}[f_0^j](x) = \Phi_{x_j}(x, 0), \quad x \in \partial G_0,$$

with discrepancy $\epsilon > 0$. Then the density function $(f^1, f^2)^T$ given by

$$(3.6) \quad \begin{pmatrix} f^1(d) \\ f^2(d) \end{pmatrix} := \mathbb{M} \begin{pmatrix} f_0^1(\mathbb{M}^{-1}d) \\ f_0^2(\mathbb{M}^{-1}d) \end{pmatrix} e^{-i\kappa d \cdot z_0}$$

satisfies

$$(3.7) \quad \|\mathbb{H}[(f^1, f^2)^T](\tilde{x}) - (\Phi_{\tilde{x}_1}, \Phi_{\tilde{x}_2})^T(\tilde{x}, z_0)\|_{L^2(\partial G)}^2 \leq 2\epsilon^2.$$

Proof. Using the transform relation, we have $\tilde{x} = \mathbb{M}x + z_0$. Since $|\tilde{x} - z_0| = |\mathbb{M}x| = |x|$, it is easy to show that

$$(3.8) \quad \begin{pmatrix} \Phi_{\tilde{x}_1}(\tilde{x}, z_0) \\ \Phi_{\tilde{x}_2}(\tilde{x}, z_0) \end{pmatrix} = \mathbb{M} \begin{pmatrix} \Phi_{x_1}(x, 0) \\ \Phi_{x_2}(x, 0) \end{pmatrix}.$$

Using (3.6), (3.8), and the property of the orthogonal transform, we get the following estimate:

$$\begin{aligned} & \|\mathbb{H}[f^1](\cdot) - \Phi_{\tilde{x}_1}(\cdot, z_0)\|_{L^2(\partial G)}^2 = \int_{\partial G} \left| \int_{\mathbb{S}} e^{i\kappa \tilde{x} \cdot d} g^1(d) ds(d) - \Phi_{\tilde{x}_1}(\tilde{x}, z_0) \right|^2 ds(\tilde{x}) \\ &= \int_{\partial G_0} \left| \int_{\mathbb{S}} e^{i\kappa z_0 \cdot d} e^{i\kappa x \cdot \mathbb{M}^{-1}d} f^1(d) ds(d) - (m_{11}\Phi_{x_1}(x, 0) + m_{12}\Phi_{x_2}(x, 0)) \right|^2 ds(x). \end{aligned}$$

Letting $\mathbb{M}^{-1}d = \tilde{d}$ and using the definition (3.6), we are led to

$$\begin{aligned} & \|\mathbb{H}[f^1](\cdot) - \Phi_{\tilde{x}_1}(\cdot, z_0)\|_{L^2(\partial G)}^2 \\ &= \int_{\partial G_0} \left| \int_{\mathbb{S}} e^{i\kappa z_0 \cdot \mathbb{M}\tilde{d}} e^{i\kappa x \cdot \tilde{d}} f^1(\mathbb{M}\tilde{d}) ds(\tilde{d}) - \sum_{j=1}^2 m_{1j}\Phi_{x_j}(x, 0) \right|^2 ds(x) \\ &= \sum_{j=1}^2 m_{1j}^2 \int_{\partial G_0} \left| \int_{\mathbb{S}} e^{i\kappa x \cdot \tilde{d}} f_0^j(\tilde{d}) ds(\tilde{d}) - \Phi_{x_j}(x, 0) \right|^2 ds(x) \\ & \quad + 2m_{11}m_{12} \int_{\partial G_0} \prod_{j=1}^2 \left[\int_{\mathbb{S}} e^{i\kappa x \cdot \tilde{d}} f_0^j(\tilde{d}) ds(\tilde{d}) - \Phi_{x_j}(x, 0) \right] ds(x) \\ & \leq \epsilon^2 + 2m_{11}m_{12} \int_{\partial G_0} \prod_{j=1}^2 \left[\int_{\mathbb{S}} e^{i\kappa x \cdot \tilde{d}} f_0^j(\tilde{d}) ds(\tilde{d}) - \Phi_{x_j}(x, 0) \right] ds(x) \end{aligned}$$

using $m_{11}^2 + m_{12}^2 = 1$ and the definition of f_0^j . In a similar way, we get that

$$\begin{aligned} & \|\mathbb{H}[f^2](\cdot) - \Phi_{\tilde{x}_2}(\cdot, z_0)\|_{L^2(\partial G)}^2 \\ & \leq \epsilon^2 + 2m_{21}m_{22} \int_{\partial G_0} \prod_{j=1}^2 \left[\int_{\mathbb{S}} e^{i\kappa x \cdot \tilde{d}} f_0^j(\tilde{d}) ds(\tilde{d}) - \Phi_{x_j}(x, 0) \right] ds(x). \end{aligned}$$

Noticing that $m_{11}m_{12} + m_{21}m_{22} = 0$, we finally get (3.7) by summing up these two estimates. The proof is complete. \square

Compared with Lemma 3.1, this result is its generalization in some weak sense; that is, we cannot assert $(f^1(d), f^2(d))$ is the minimum norm solution of

$$(3.9) \quad \mathbb{H}[(\varphi^1, \varphi^2)^T](\tilde{x}) = (\Phi_{\tilde{x}_1}, \Phi_{\tilde{x}_2})^T(\tilde{x}, z_0), \quad \tilde{x} \in \partial G,$$

with discrepancy $\sqrt{2}\epsilon$. Fortunately, such a weak generalization is enough for our purpose. On the other hand, the discrepancy level $\sqrt{2}\epsilon$ is optimal for the density function given by (3.6).

A small change of the assumptions on $f_0^j(d)$ can guarantee that $(f^1(d), f^2(d))$ is the minimum norm solution of (3.9). This is the following analogy of Lemma 3.1.

THEOREM 3.3. *Assume that the vector-valued function $(f_0^1(d), f_0^2(d)) \in L^2(\mathbb{S} \times \mathbb{S})$ is the minimum norm solution of*

$$(3.10) \quad \mathbb{H}[(\varphi^1, \varphi^2)^T](x) = (\Phi_{x_1}, \Phi_{x_2})^T(x, 0), \quad x \in \partial G_0,$$

with discrepancy $\epsilon > 0$. Then the density function $(f^1, f^2)^T$ given by (3.6) is the minimum norm solution of (3.9) with discrepancy $\epsilon > 0$.

Proof. The computation in the proof of the above theorem yields that

$$\left\{ \begin{aligned} & \|\mathbb{H}[f^1](\cdot) - \Phi_{\tilde{x}_1}(\cdot, z_0)\|_{L^2(\partial G)}^2 = \sum_{j=1}^2 m_{1j}^2 \|\mathbb{H}[f_0^j](\cdot) - \Phi_{x_j}(x, 0)\|_{L^2(\partial G_0)}^2 \\ & \quad + 2m_{11}m_{12} \int_{\partial G_0} \prod_{j=1}^2 \left[\int_{\mathbb{S}} e^{i\kappa x \cdot \tilde{d}} f_0^j(\tilde{d}) ds(\tilde{d}) - \Phi_{x_j}(x, 0) \right] ds(x), \\ & \|\mathbb{H}[f^2](\cdot) - \Phi_{\tilde{x}_2}(\cdot, z_0)\|_{L^2(\partial G)}^2 = \sum_{j=1}^2 m_{2j}^2 \|\mathbb{H}[f_0^j](\cdot) - \Phi_{x_j}(x, 0)\|_{L^2(\partial G_0)}^2 \\ & \quad + 2m_{21}m_{22} \int_{\partial G_0} \prod_{j=1}^2 \left[\int_{\mathbb{S}} e^{i\kappa x \cdot \tilde{d}} f_0^j(\tilde{d}) ds(\tilde{d}) - \Phi_{x_j}(x, 0) \right] ds(x). \end{aligned} \right.$$

Summing up these two identities and noticing $m_{11}m_{12} + m_{21}m_{22} = 0$, we get that

$$\begin{aligned} & \|\mathbb{H}[(f^1, f^2)^T](\cdot) - (\Phi_{\tilde{x}_1}, \Phi_{\tilde{x}_2})^T(\cdot, z_0)\|_{L^2(\partial G \times \partial G)}^2 \\ & = \sum_{j=1}^2 m_{1j}^2 \|\mathbb{H}[f_0^j](\cdot) - \Phi_{x_j}(\cdot, 0)\|_{L^2(\partial G_0)}^2 + \sum_{j=1}^2 m_{2j}^2 \|\mathbb{H}[f_0^j](\cdot) - \Phi_{x_j}(\cdot, 0)\|_{L^2(\partial G_0)}^2. \end{aligned}$$

Using the properties $m_{11} = m_{22}, m_{12} = -m_{21}$, and $m_{11}^2 + m_{12}^2 = 1$, the above equality becomes by exchanging the order of summation

$$\begin{aligned} & \|\mathbb{H}[(f^1, f^2)^T](\cdot) - (\Phi_{\tilde{x}_1}, \Phi_{\tilde{x}_2})^T(\cdot, z_0)\|_{L^2(\partial G \times \partial G)}^2 = \sum_{j=1}^2 \|\mathbb{H}[f_0^j](\cdot) - \Phi_{x_j}(\cdot, 0)\|_{L^2(\partial G_0)}^2 \\ & = \|\mathbb{H}[(f_0^1, f_0^2)^T](\cdot) - (\Phi_{x_1}, \Phi_{x_2})^T(\cdot, 0)\|_{L^2(\partial G_0 \times \partial G_0)}^2 \leq \epsilon^2 \end{aligned}$$

from the definition of (f_0^1, f_0^2) . That is, (f^1, f^2) is an approximate solution of (3.9) with discrepancy ϵ .

Next, we prove that $(f_1, f_2)^T$ is also the minimum norm solution of (3.9) with discrepancy ϵ . If this argument is not true, then there exists another function $(\tilde{f}_1, \tilde{f}_2) \in L^2(\mathbb{S} \times \mathbb{S})$, which is the minimum norm solution of (3.9) with discrepancy ϵ . That is, $(\tilde{f}_1, \tilde{f}_2)$ meets

$$(3.11) \quad \|\mathbb{H}[(\tilde{f}^1, \tilde{f}^2)](\cdot) - (\Phi_{\tilde{x}_1}, \Phi_{\tilde{x}_2})^T(\cdot, z_0)\|_{L^2(\partial G \times \partial G)}^2 \leq \epsilon^2$$

and

$$(3.12) \quad \|(\tilde{f}^1, \tilde{f}^2)\|_{L^2(\mathbb{S} \times \mathbb{S})}^2 < \|(f^1, f^2)\|_{L^2(\mathbb{S} \times \mathbb{S})}^2.$$

Now we construct $(\tilde{f}_0^1, \tilde{f}_0^2) \in L^2(\mathbb{S} \times \mathbb{S})$ by

$$(3.13) \quad \begin{pmatrix} \tilde{f}_0^1(d) \\ \tilde{f}_0^2(d) \end{pmatrix} := \mathbb{M}^{-1} \begin{pmatrix} \tilde{f}^1(\mathbb{M}d) \\ \tilde{f}^2(\mathbb{M}d) \end{pmatrix} e^{i\kappa \mathbb{M}d \cdot z_0}.$$

By direct computation using the transform relation and (3.11), we can derive that

$$(3.14) \quad \|\mathbb{H}[(\tilde{f}_0^1, \tilde{f}_0^2)](\cdot) - (\Phi_{x_1}, \Phi_{x_2})^T(\cdot, z_0)\|_{L^2(\partial G_0 \times \partial G_0)}^2 \leq \epsilon^2.$$

On the other hand, using the definitions (3.6) and (3.13), we can prove that

$$\|(\tilde{f}_0^1, \tilde{f}_0^2)^T\|_{L^2(\mathbb{S} \times \mathbb{S})} = \|(\tilde{f}^1, \tilde{f}^2)^T\|_{L^2(\mathbb{S} \times \mathbb{S})}, \quad \|(f_0^1, f_0^2)^T\|_{L^2(\mathbb{S} \times \mathbb{S})} = \|(f^1, f^2)^T\|_{L^2(\mathbb{S} \times \mathbb{S})}.$$

Therefore (3.12) yields

$$(3.15) \quad \|(\tilde{f}_0^1, \tilde{f}_0^2)^T\|_{L^2(\mathbb{S} \times \mathbb{S})}^2 < \|(f_0^1, f_0^2)^T\|_{L^2(\mathbb{S} \times \mathbb{S})}^2.$$

Combining (3.14) and (3.15), we conclude that $(f_0^1, f_0^2)^T$ is not the minimum norm solution of (3.10) with discrepancy ϵ , which is a contradiction. \square

Comparing Theorems 3.2 and 3.3, both of them can be used to construct the approximation of $\Phi_{x_j}(\tilde{x}, z_0)$ in ∂G from the minimum norm solution in the reference domain ∂G_0 . However, in order to guarantee that (f^1, f^2) is the minimum norm solution, we need to solve the density (f_0^1, f_0^2) as the minimum norm solution from the coupled equation (3.10), which will lead to a large amount of computation since \mathbb{H} is defined in $L^2(\mathbb{S}) \times L^2(\mathbb{S})$ in this case. Therefore, from the numerical point of view, Theorem 3.2 is more suitable for the approximation.

For the second derivative of the fundamental solution, we have similar results.

THEOREM 3.4. *Assume that $h_0^j(d)$ with $j = 1, 2$ are minimum norm solutions of*

$$(3.16) \quad \mathbb{H}[h_0^j](x) = \Phi_{x_j x_2}(x, 0), \quad x \in \partial G_0,$$

with discrepancy $\epsilon > 0$. Then the density function $(h^1, h^2)^T$ given by

$$(3.17) \quad \begin{pmatrix} h^1(d) \\ h^2(d) \end{pmatrix} := \mathbb{M}^2 \begin{pmatrix} h_0^1(\mathbb{M}^{-1}d) \\ h_0^2(\mathbb{M}^{-1}d) \end{pmatrix} e^{-i\kappa d \cdot z_0} - \mathbb{M} \begin{pmatrix} \kappa^2 m_{21} \\ 0 \end{pmatrix} g(\mathbb{M}^{-1}d) e^{-i\kappa d \cdot z_0}$$

satisfies

$$(3.18) \quad \|\mathbb{H}[(h^1, h^2)^T](\cdot) - (\Phi_{\tilde{x}_1 \tilde{x}_2}, \Phi_{\tilde{x}_2 \tilde{x}_2})^T(\cdot, z_0)\|_{L^2(\partial G \times \partial G)}^2 \leq (2 + \kappa^2)\epsilon^2.$$

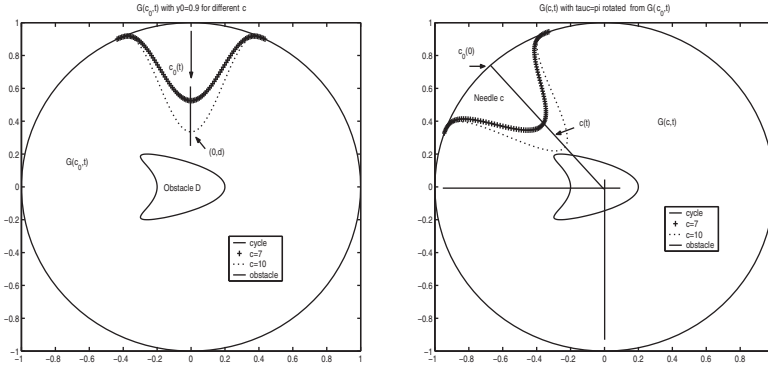


FIG. 3.1. A possible configuration of reference domain D_0 (left) and its rigid transform by rotation and translation (right).

Proof. It follows from (3.8) and the fact that $\Phi_{x_1x_1}(x, 0) + \Phi_{x_2x_2}(x, 0) \equiv -\kappa^2\Phi(x, 0)$ that

$$\begin{aligned}
 \begin{pmatrix} \Phi_{\tilde{x}_1\tilde{x}_2}(\tilde{x}, z_0) \\ \Phi_{\tilde{x}_2\tilde{x}_2}(\tilde{x}, z_0) \end{pmatrix} &= \mathbb{M} \frac{\partial}{\partial \tilde{x}_2} \begin{pmatrix} \Phi_{x_1}(x, 0) \\ \Phi_{x_2}(x, 0) \end{pmatrix} \\
 &= \mathbb{M} \begin{pmatrix} \frac{\partial x_2}{\partial \tilde{x}_2} & -\frac{\partial x_1}{\partial \tilde{x}_2} \\ \frac{\partial x_1}{\partial \tilde{x}_2} & \frac{\partial x_2}{\partial \tilde{x}_2} \end{pmatrix} \begin{pmatrix} \Phi_{x_1x_2}(x, 0) \\ \Phi_{x_2x_2}(x, 0) \end{pmatrix} - \mathbb{M} \begin{pmatrix} \kappa^2 m_{21} \\ 0 \end{pmatrix} \Phi(x, 0) \\
 (3.19) \quad &= \mathbb{M}^2 \begin{pmatrix} \Phi_{x_1x_2}(x, 0) \\ \Phi_{x_2x_2}(x, 0) \end{pmatrix} - \mathbb{M} \begin{pmatrix} \kappa^2 m_{21} \\ 0 \end{pmatrix} \Phi(x, 0).
 \end{aligned}$$

Now the proof is the same as that of Theorem 3.2 in treating the first term and applying Lemma 3.1 for the second term in (3.19), noticing \mathbb{M}^2 is also orthogonal and $|m_{21}| \leq 1$. \square

From the above results, we get the following corollary.

COROLLARY 3.5. Assume that g_0 , f_0^j , and h_0^j are the minimum norm solutions of (3.1), (3.5), and (3.16) with discrepancy ϵ in the fixed reference domain ∂G_0 , respectively. Then the density functions g , f^j , and h^j constructed by (3.3), (3.6), and (3.17), respectively, meet

$$(3.20) \quad \|\mathbb{H}[g] - \Phi(\cdot, z_0)\| \leq \epsilon, \quad \|\mathbb{H}[f^j] - \Phi_{x_j}(\cdot, z_0)\| \leq \sqrt{2}\epsilon, \quad \|\mathbb{H}[h^j] - \Phi_{x_jx_2}(\cdot, z_0)\| \leq \sqrt{2 + \kappa^2}\epsilon$$

for $j = 1, 2$, where the norm is in $L^2(\partial G)$ and $G = \mathbb{M}G_0 + z_0$.

Using this result, we can approximate the singular source by Herglotz wave functions in all approximate domains $\partial D_a^p := \mathbb{M}(a)D_0 + z_p$ with a small amount of computations, where $\mathbb{M}(a)$ represents the approaching direction and z_p the approaching step along this direction. When we choose different rotation matrix $\mathbb{M}(a)$ and approaching points z_p from a fixed reference domain D_0 , $z_p \notin D_a^p$ can approach any points $a \in \partial D$. Once we compute the minimum norm solution φ_0 in the fixed reference domain ∂D_0 , the density functions for approaching the singular source in ∂D_a^p can be computed from φ_0 by a simple function transformation. Using this method, the numerical realizations of the probe method can be implemented efficiently. A geometric configuration of the reference domain D_0 with some cone shaped boundary and its transform are shown in Figure 3.1.

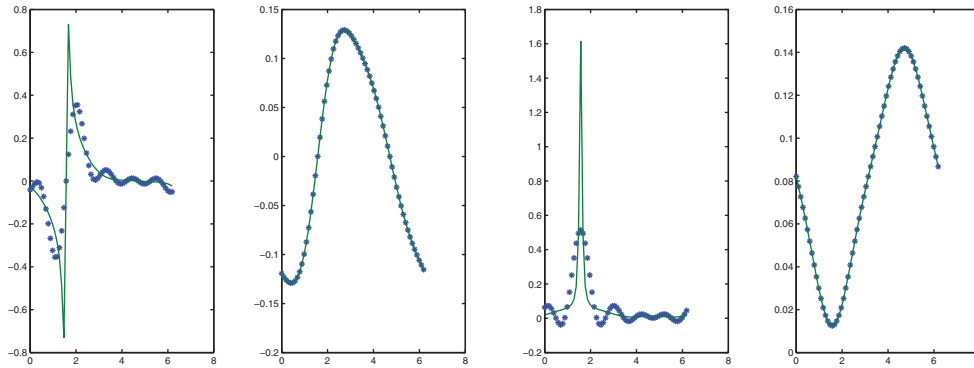


FIG. 4.1. The singular behaviors of $\Phi_{x_1}(x, z_0)$ (first and second graphs) and $\Phi_{x_2}(x, z_0)$ (third and fourth graphs) in a circle $|x| = R_0$ with $z_0 = (0, R_0 + \delta_0)$ for small δ_0 , together with their approximations shown in star line using uniform mesh. The imaginary parts of $\Phi_{x_i}(x, z_0)$ are quite smooth and therefore can be approximated well.

4. Error estimates on the singular source approximation. When we decompose the singular sources such as $\Phi(x, z_p)$, $\partial_{x_j}\Phi(x, z_p)$, and $\partial_{x_j x_2}\Phi(x, z_p)$ with $j = 1, 2$ approximately into the superposition of incident plan waves in ∂D_a^p , we need to solve an integral equation of the first kind

$$(4.1) \quad \mathbb{H}[\varphi](x) = F(x, 0), \quad x \in \partial G_0,$$

in the boundary of reference domain G_0 , where we assume that $0 \notin \overline{G_0}$ and $F(x, 0)$ represent $\Phi(x, 0)$, $\partial_{x_j}\Phi(x, 0)$, or $\partial_{x_j x_2}\Phi(x, 0)$. The theoretical results in section 3 assert that the approximation accuracy in every approximate domain ∂D_a^p is essentially determined by the solution (4.1), since the function transform for the density with an analytic expression does not generate extra error. Notice that (4.1) may not have an exact solution even for exact $F(x, 0)$. This fact means that we must yield some approximate solution in the sense that (4.1) holds approximately.

Compared with the general integral equation of the first kind, the difficulty in solving (4.1) by regularization is that the right-hand side of (4.1) is almost a singular function for $x \in \partial G_0$ near 0, in the sense that the real part of $F(x, 0)$ has a very sharp peak near point 0; see Figure 4.1. Therefore we need to estimate the influence of such a sharp peak on the numerical solution. More precisely, the relation between this peak strength of $F(x, 0)$, the choice of regularizing parameter α , and the discrete number n for dividing ∂G_0 and \mathbb{S} in solving (4.1) should be analyzed.

The minimum norm solution $\varphi_\epsilon(d)$ of (4.1) with discrepancy $\epsilon > 0$ is obtained by solving the equation

$$(4.2) \quad \alpha\varphi^\alpha(d) + \mathbb{H}^*\mathbb{H}[\varphi^\alpha](d) = \mathbb{H}^*[F](d), \quad d \in \mathbb{S},$$

where the regularizing parameter $\alpha = \alpha(\epsilon)$ may be determined by the Morozov discrepancy principle

$$(4.3) \quad \|\mathbb{H}[\varphi^\alpha](\cdot) - F(\cdot, 0)\|_{L^2(\partial G_0)} = \epsilon.$$

That is, $\varphi_\epsilon = \varphi^{\alpha(\epsilon)}$ with $\varphi^{\alpha(\epsilon)}$ determined from (4.2) and (4.3). We need to estimate $\|\mathbb{H}[\varphi_{\epsilon, N}] - F\|_{L^2(\partial G_0)}$, where $\varphi_{\epsilon, N}$ is the finite dimensional approximation to $\varphi_\epsilon \in L^2(\mathbb{S})$.

Introduce the finite dimensional subspace $X_n \subset L^2(\mathbb{S}), Y_n \subset L^2(\partial G_0)$. Denote by φ_n, F_n the projection of $\varphi \in L^2(\mathbb{S}), F \in L^2(\partial G_0)$ into X_n, Y_n , respectively. Then, for any fixed $\alpha > 0$, it is well-known for the regularizing equation (4.2) that

$$(4.4) \quad \|\varphi_n^\alpha - \varphi^\alpha\|_{L^2(\mathbb{S})} \leq \frac{1}{2\sqrt{\alpha}} \|F_n - F\|_{L^2(\partial G_0)}.$$

Therefore the approximation to the density function with minimum norm meets

$$(4.5) \quad \|\varphi_{\epsilon,n} - \varphi_\epsilon\|_{L^2(\mathbb{S})} \leq \frac{1}{2\sqrt{\alpha(\epsilon)}} \|F_n - F\|_{L^2(\partial G_0)}.$$

Finally, we have the estimate

$$(4.6) \quad \begin{aligned} \|\mathbb{H}[\varphi_{\epsilon,N}] - F\|_{L^2(\partial G_0)} &\leq \|\mathbb{H}[\varphi_{\epsilon,n} - \varphi_\epsilon]\|_{L^2(\partial G_0)} + \|\mathbb{H}[\varphi_\epsilon] - F\|_{L^2(\partial G_0)} \\ &\leq \|\mathbb{H}\|_{L^2} \frac{1}{2\sqrt{\alpha(\epsilon)}} \|F_n - F\|_{L^2(\partial G_0)} + \epsilon. \end{aligned}$$

This estimate reveals that the approximation accuracy of the singular source function by the Herglotz wave function in a finite dimensional space depends on the balance of $\frac{1}{2\sqrt{\alpha(\epsilon)}} \|F_n - F\|_{L^2(\partial G_0)}$ and ϵ . We state the above analysis as the following theorem.

THEOREM 4.1. *Assume that $\|F(\cdot, 0)\|_{L^2(\partial G_0)} > \epsilon$ and $\alpha(\epsilon)$ is the regularizing parameter related to the minimum norm solution of (4.1) with discrepancy ϵ . If the dimension $n := n(\epsilon)$ is chosen to meet*

$$(4.7) \quad \|F_n - F\|_{L^2(\partial G_0)} = O(\epsilon\sqrt{\alpha(\epsilon)}),$$

then the error for the singular source approximation using the Herglotz wave function with the density function in finite dimensional space X_n satisfies the estimate

$$\|\mathbb{H}[\varphi_{\epsilon,n}] - F\|_{L^2(\partial G_0)} = O(\epsilon) \text{ as } \epsilon \rightarrow 0.$$

This estimate gives us a theoretical criterion for taking the dimension of the approximate function subspace. From the standard estimate [16]

$$(4.8) \quad 0 < \alpha(\epsilon) \leq \frac{\|\mathbb{H}^*\| \epsilon}{\|F(\cdot, 0)\|_{L^2(\partial G_0)} - \epsilon},$$

we know that $\alpha(\epsilon) \rightarrow 0$ at least linearly with respect to ϵ . Therefore we need to choose the dimension $n = n(\epsilon)$ of projection subspace Y_n to satisfy at least $\|F_n - F\|_{L^2(\partial G_0)} = O(\epsilon^{3/2})$ to guarantee the approximation. Noticing that the smoothness of $F(x, 0)$ is not uniform in ∂G_0 , see Figure 4.1, it is preferable to take nonuniform mesh to meet this requirement. If uniform mesh is taken, then n must be quite large for small ϵ .

To determine the exact $\alpha(\epsilon)$, we need to solve a nonlinear equation constituted by (4.2) and (4.3), which is time-consuming. However, our numerical experiences show that a rough choice

$$\alpha(\epsilon) := \frac{\beta \|\mathbb{H}^*\| \epsilon}{\|F(\cdot, 0)\|_{L^2(\partial G_0)} - \epsilon}$$

for fixed $\beta \in (0, 1)$ is applicable for our singular source approximation. In fact, in numerical implementations given in the next section, we take $\beta = 10^{-l}$ with $l = 1, 2, 3$

and choose one of them such that $H[\varphi^\alpha](x)$ approximates $F(x, 0)$ with minimum discrepancy.

Since the probe method uses the singularity of the fundamental solution in the pointwise sense to detect the obstacle boundary, we need to estimate the approximation error $\mathbb{H}[\varphi_{\epsilon,n}](x) - F(x, 0)$ in the finite dimensional space in the L^∞ -sense. Of course, this error depends on the error $\|F_n - F\|_{L^\infty}$. We give this dependence by the following theorem.

THEOREM 4.2. *Assume that $\|F(\cdot, 0)\|_{L^2(\partial G_0)} > \epsilon$ and $\alpha(\epsilon)$ is the regularizing parameter related to the minimum norm solution of (4.1) with discrepancy ϵ . Then the L^∞ -error for the singular source approximation using the density function in finite dimensional space X_n satisfies*

$$(4.9) \quad \left| \|\mathbb{H}[\varphi_{\epsilon,n}] - F\|_{L^\infty(\partial G_0)} - \|\mathbb{H}[\varphi_\epsilon] - F\|_{L^\infty(\partial G_0)} \right| < \frac{C_0}{\sqrt{\alpha(\epsilon)^3}} \|F_n - F\|_{L^\infty(\partial G_0)},$$

where the constant $C_0 = \|\mathbb{H}\|_\infty \|\mathbb{H}^*\|_\infty (\sqrt{|\partial G_0| |\mathbb{S}|} + 2) / \sqrt{2}$.

Proof. Using the triangle inequality, it follows that

$$(4.10) \quad \begin{aligned} \|\mathbb{H}[\varphi_{\epsilon,n}] - F\|_{L^\infty(\partial G_0)} &\leq \|\mathbb{H}[\varphi_{\epsilon,n} - \varphi_\epsilon]\|_{L^\infty(\partial G_0)} + \|\mathbb{H}[\varphi_\epsilon] - F\|_{L^\infty(\partial G_0)} \\ &\leq \|\mathbb{H}\|_\infty \|\varphi_{\epsilon,n} - \varphi_\epsilon\|_{L^\infty(\mathbb{S})} + \|\mathbb{H}[\varphi_\epsilon] - F\|_{L^\infty(\partial G_0)}. \end{aligned}$$

Now let us estimate $\|\varphi_{\epsilon,n} - \varphi_\epsilon\|_{L^\infty(\mathbb{S})}$. Define $\psi_n(d) := \varphi_{\epsilon,n}(d) - \varphi_\epsilon(d)$ and $f_n(x) := F_n(x, 0) - F(x, 0)$ for simplicity of notation. It is easy to see that

$$(4.11) \quad \alpha \psi_n(d) + \mathbb{H}^* \mathbb{H}[\psi_n](d) = \mathbb{H}^*[f_n](d), \quad d \in \mathbb{S},$$

which means that

$$(4.12) \quad \|\psi_n\|_{L^\infty(\mathbb{S})} \leq \|(\alpha \mathbb{I} + \mathbb{H}^* \mathbb{H})^{-1} \mathbb{H}^*\|_\infty \|f_n\|_{L^\infty(\partial G_0)}.$$

We claim that

$$(4.13) \quad \|(\alpha \mathbb{I} + \mathbb{H}^* \mathbb{H})^{-1} \mathbb{H}^*\|_\infty \leq \frac{\|\mathbb{H}^*\|_\infty (\sqrt{|\partial G_0| |\mathbb{S}|} + 2)}{2\sqrt{\alpha^3}}$$

for $\alpha \in (0, 1)$. In fact, assume that $(\alpha \mathbb{I} + \mathbb{H}^* \mathbb{H})^{-1} \mathbb{H}^* w = \psi$ in \mathbb{S} ; then it follows from the standard estimate of the Tikhonov regularization in L^2 setting that

$$\|\psi\|_{L^2(\mathbb{S})} \leq \|(\alpha \mathbb{I} + \mathbb{H}^* \mathbb{H})^{-1} \mathbb{H}^*\|_{L^2} \|w\|_{L^2(\partial G_0)} \leq \frac{\sqrt{|\partial G_0|}}{2\sqrt{\alpha}} \|w\|_\infty.$$

On the other hand, we get from $(\alpha \mathbb{I} + \mathbb{H}^* \mathbb{H})\psi = \mathbb{H}^* w$ that

$$\|\psi\|_\infty \leq \frac{1}{\alpha} [\|\mathbb{H}^* w\|_\infty + \|\mathbb{H}^* \mathbb{H} \psi\|_\infty] \leq \frac{\|\mathbb{H}^*\|_\infty}{\alpha} [\|w\|_\infty + \|\mathbb{H} \psi\|_\infty].$$

From the definition of \mathbb{H} , it is easy to see that

$$|\mathbb{H}[\psi](x)| \leq \int_{\mathbb{S}} |e^{i\kappa d \cdot x} \psi(d)| ds(d) \leq \sqrt{|\mathbb{S}|} \|\psi\|_{L^2(\mathbb{S})}.$$

The above three estimates lead to (4.13).

Inserting (4.13) and (4.12) into (4.10), we obtain

$$\|\mathbb{H}[\varphi_{\epsilon,n}] - F\|_{L^\infty(\partial G_0)} \leq \frac{C_0}{\sqrt{\alpha(\epsilon)^3}} \|f_n\|_{L^\infty} + \|\mathbb{H}[\varphi_\epsilon] - F\|_{L^\infty(\partial G_0)}.$$

Exchanging the position of $\varphi_{\epsilon,n}$ and φ_ϵ in this relation and combining these two relations together, the proof is complete. \square

Remark 4.3. The fact that the discrete error $\|\mathbb{H}[\varphi_{\epsilon,n}] - F\|_{L^\infty(\partial G_0)}$ depends on its continuous version $\|\mathbb{H}[\varphi_\epsilon] - F\|_{L^\infty(\partial G_0)}$ is obvious. The importance of this theorem is the relation of these two terms. Compared with the L^2 -norm estimate given in the previous theorem, this theorem states that we need to take a larger $n := n(\epsilon)$ to get the same error as that of the measurement by the L^2 -norm. It is generally impossible to estimate $\|\mathbb{H}[\varphi_{\epsilon,n}] - F\|_{L^\infty(\partial G_0)}$ by ϵ explicitly, since we have only the estimate $\|\mathbb{H}[\varphi_\epsilon] - F\|_{L^2(\partial G_0)} < \epsilon$.

5. Numerical implementations. We give the numerics to test the algorithm. In all the numerical tests, we take wave number $\kappa = 1.2$ and use far field pattern data along 64 directions. The detection of the obstacle boundary is also along 64 directions uniformly distributed in $[0, 2\pi]$.

As a first effort in the numerical realization of our higher order expansion formula, here we focus on the effect of surface impedance and the obstacle curvature by using (2.20) to detect the boundary. The realizations for (2.25), (2.26), and (2.27) in reconstructing the surface impedance will be given in the sequel paper.

Example 1. Take D to be a cycle

$$\partial D := \{x = 1.5 \times (\cos t, \sin t), t \in [0, 2\pi]\}.$$

Step 1. First we choose the surface impedance as a real constant. For this special case with a constant curvature, we consider the case that ∂D has a mixed boundary $\partial D_D = \{x \in \partial D : t \in [0, \pi]\}$ and $\partial D_I = \{x \in \partial D : t \in (\pi, 2\pi]\}$.

We take singularity $\delta_1 = 0.01$ and the approaching steps $\delta_0 = 0.02$ for $l = 16, \dots, 1$. That is, along each direction, the approaching radius is $1.5 + l \times \delta_0 + \delta_1$.

The results for $\sigma(x) = 30$ and $\sigma(x) = 3$ using the same blowing-up criterion in all directions are shown in Figure 5.1. For large σ (left), which implies the impedance boundary is almost a Dirichlet boundary, the whole obstacle is detected well; see the

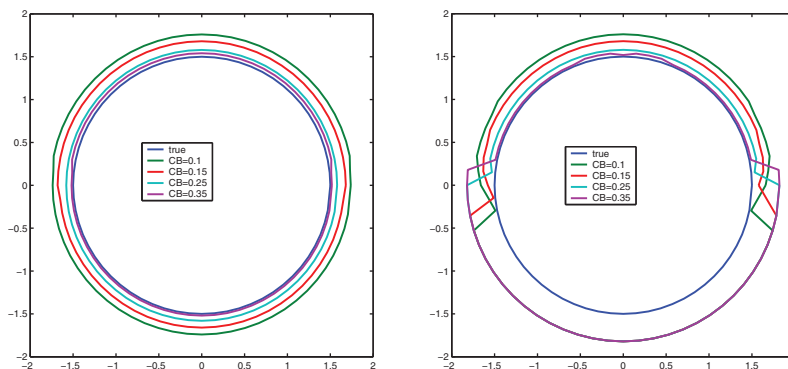


FIG. 5.1. Reconstruction of ∂D for the mixed boundary condition with $\sigma(x) = 30$ (left) and $\sigma(x) = 3$ (right) in ∂D_I , using the uniform blowing-up criteria in all directions.

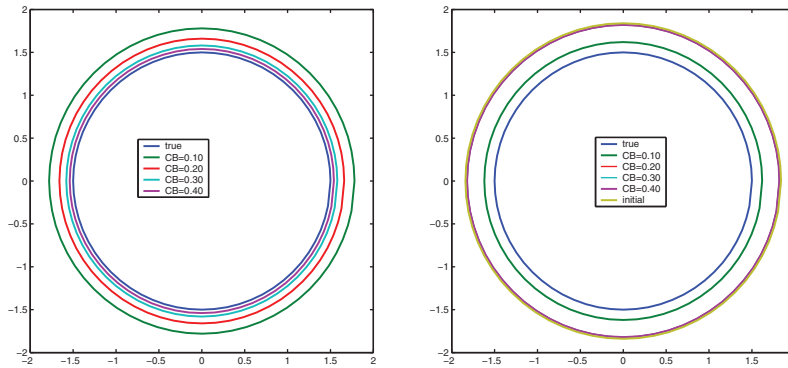


FIG. 5.2. Reconstruction of ∂D for surface impedance in ∂D with $\sigma(x) = 5 - 5i$ (left) and $\sigma(x) = 5 - \frac{0.6667}{2 \times 1.2}i$ (right), using the uniform blowing-up criteria in all directions. For large blowing-up values, the boundary cannot be seen (right).

first picture in Figure 5.1. However, for small $\sigma(x)$ (right), the blowing-up behavior for the impedance boundary is weak. Using the same blowing-up criterion in all directions, the impedance part cannot be detected; that is, all detection points of the impedance boundary are just the initial guess; see the second picture in Figure 5.1. These numerical tests reveal that the same blowing-up criterion cannot be used for the mixed boundary condition, provided that $\sigma^r(x)$ is not very large.

Step 2. To explain the effect of surface impedance in the whole boundary clearly, we assume $\partial D = \partial D_I$ and consider three cases:

$$\sigma(x) = 5 - 5i, \quad \sigma(x) = 5 - \frac{0.6667}{2\kappa}i, \quad \sigma(x) = 5 - 5 \sin(6x_1x_2)i$$

distributed in the whole boundary. The second case meets $\frac{1}{2}\mathcal{C}(a) + \kappa\sigma^i(a) \equiv 0$ in ∂D_I . Notice that it has been shown in Step 1 that the blowing-up criterion cannot be chosen as the same value in all directions for the mixed boundary condition.

We take $\delta_0 = \delta_1 = 0.02$. Using different uniform blowing-up values, the reconstructions are given in Figure 5.2 for the first two configurations. We see that the whole obstacle can be seen for both cases. However, the reconstruction is better in the picture on the left-hand side. This is natural, and it can be explained using (2.28). Indeed, for the picture on the left-hand side, we have $\frac{1}{2}\mathcal{C}(a) + \kappa\sigma^i(a) = -5\kappa + 0.6667/2$ on ∂D which is negative and therefore decreases the value of the first term in (2.28), while for the picture on the right-hand side we have $\frac{1}{2}\mathcal{C}(a) + \kappa\sigma^i(a) = 0$ on ∂D . For this reason, the detecting point z_p must be closer to ∂D than that in the right-hand picture for the same suitable blowing-up value. As a result, the reconstruction is better in the left-hand side picture. However, the blowup is mostly uniform for both pictures since we have the uniform curvature for a circle and constant value $\frac{1}{2}\mathcal{C}(a) + \kappa\sigma^i(a)$.

The reconstructions with oscillatory $\sigma^i(x)$ (the third case) are shown in Figure 5.3. It can be seen that the oscillation of $\sigma^i(x)$ on ∂D makes the reconstruction of the obstacle less accurate. In addition, for large blowing-up values of CB , we cannot recognize at all the very well uniform shape of a circle. It is worth noticing that this phenomenon should be the same using any of the indicator functions $I^0, I_j^i, i, j = 1, 2$, or even using indicators based on multipoles of higher orders.

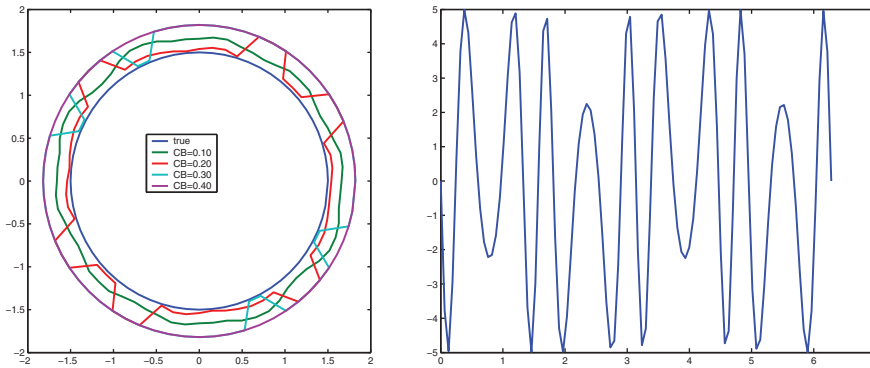


FIG. 5.3. Reconstruction of ∂D for surface impedance with oscillatory imaginary part (left) and the function $\text{Im } \sigma(x)$ (right). The formula (2.20) can be used to explain this reconstruction. That is, the oscillation of $\sigma^i(x)$ in ∂D_I decreases the visibility of the obstacle.

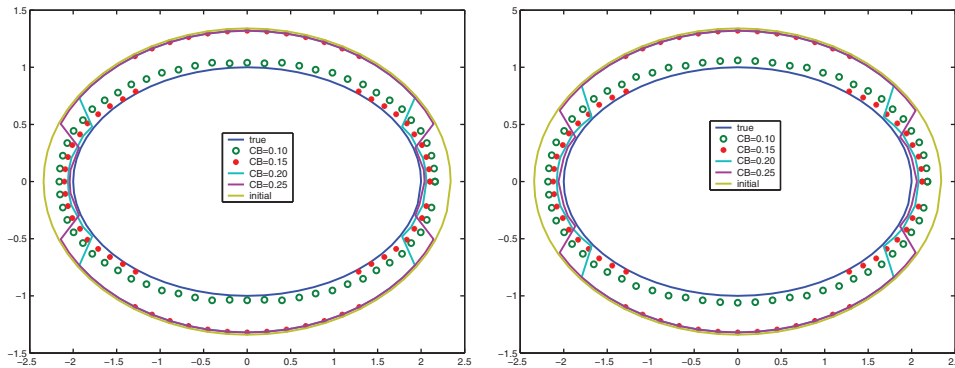


FIG. 5.4. Reconstructions for $\sigma^i(x) \equiv 0$ (left) and for the variable imaginary surface satisfying $\frac{1}{2}\mathcal{C}(x) + \kappa\sigma^i(x) \equiv 0$ in ∂D (right).

Next, we consider a convex obstacle with a varying curvature.

Example 2. Take D to be an ellipse $\partial D := \{x = (2 \cos t, \sin t), t \in [0, 2\pi]\}$, and assume that on ∂D we have a surface impedance boundary.

We show that this obstacle will be more visible by introducing suitable complex variable surface impedance $\sigma(x) = 5 + \sigma^i(x)i$.

To compare the results, we take the same values $\delta_0 = 0.02$ and $\delta_1 = 0.01$ for the singularity and use the same blowing-up criteria $CB = 0.10, 0.15, 0.20, 0.25$ for different surface impedance. Denote by

$$\mathcal{C}(x) := \frac{x'_1(t)x''_2(t) - x''_1(t)x'_2(t)}{(x'_1(t)^2 + x'_2(t)^2)^{3/2}}$$

the curvature of ∂D at point $x = x(t) \in \partial D$.

The reconstructions for the configurations $\sigma^i(x) \equiv 0$ and $\frac{1}{2}\mathcal{C}(x) + \kappa\sigma^i(x) = 0$ are given in Figure 5.4, while the reconstructions for $\frac{1}{2}\mathcal{C}(x) + \kappa\sigma^i(x) = -3$ and $\frac{1}{2}\mathcal{C}(x) + \kappa\sigma^i(x) = -10$ are given in Figure 5.5.

Although the two figures in Figure 5.4 look close due to the small curvature variance in ∂D , there are still some differences between them. For example, by in-

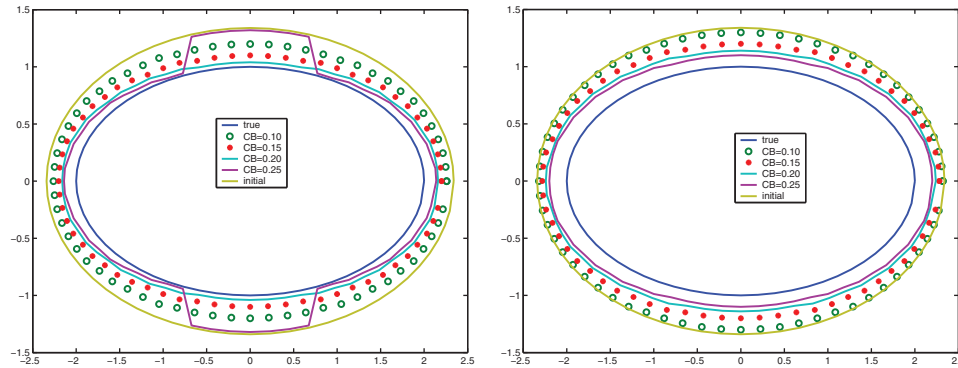


FIG. 5.5. Reconstructions for the variable imaginary surface satisfying $\frac{1}{2}\mathcal{C}(x) + \kappa\sigma^i(x) \equiv -3$ (left) and $\frac{1}{2}\mathcal{C}(x) + \kappa\sigma^i(x) \equiv -10$ (right) in ∂D .

roducing the complex impedance $\sigma^i(x)$ in terms of the curvature (right picture), the reconstruction accuracy for large curvature part for the same blowing up value has been improved. Comparing the reconstruction behaviors presented in Figures 5.4 and 5.5, we can see clearly how the introduction of the imaginary part of surface impedance makes the obstacle more uniformly visible step by step. That is, in the right-hand side of Figure 5.5, the good accuracy near $t = 0$ and $t = \pi$ due to the large curvature has been relatively weakened, or equivalently, the accuracy near $t = \pi/2$ and $t = 3\pi/2$ is relatively improved. The whole boundary has a uniform visibility. That is, all points of the boundary are reconstructed with almost the same accuracy. Notice that, using the largest blowing-up value $CB = 0.25$ with $\sigma^i(x) \equiv 0$, it can detect the small part with largest curvature (near $t = 0, \pi$) almost exactly, but we see nothing in the other part. However, when we introduce $\frac{1}{2}\mathcal{C}(x) + \kappa\sigma^i(x) \equiv -10$, the same blowing-up value can detect the whole boundary uniformly, with a cost of relatively small accuracy in the part with largest curvature. Moreover, it is also the better reconstruction compared with the other small indicator value shown in the second picture of Figure 5.5. This can be explained in the same way as we did for Figure 5.3 using (2.28).

Example 3. Consider a complex obstacle

$$\partial D = \{x : x(t) = (x_1(t), x_2(t)) = (\cos t + 0.65 \cos 2t - 0.65, 1.5 \sin t), t \in [0, 2\pi]\},$$

which contains a concave part and a large oscillation of the curvature. The obstacle as well as its curvature distribution are shown in Figure 5.6.

Step 1. We consider the constant surface impedance using the approaching parameters $\delta_0 = \delta_1 = 0.02$. The reconstruction for $\sigma(x) = 5$ and $\sigma(x) = 5 - 5i$ are shown in Figure 5.7.

Of course, the blowing-up criterion is not uniform in all directions for this configuration, since the impedance is constant and the geometric shape has essential differences in the different parts of the boundary. This phenomena is revealed in the reconstruction. For the same blowing-up value, the best reconstructions are obtained near A and B due to the large curvature and therefore the strong scattering. Obviously, if large blowing-up values ($CB = 0.2, 0.3, 0.4$) are given, then most of the boundary part with small curvature cannot be reconstructed due to weak scattering. On the other hand, the introduction of the constant imaginary part improves the uniform property but not satisfactorily.

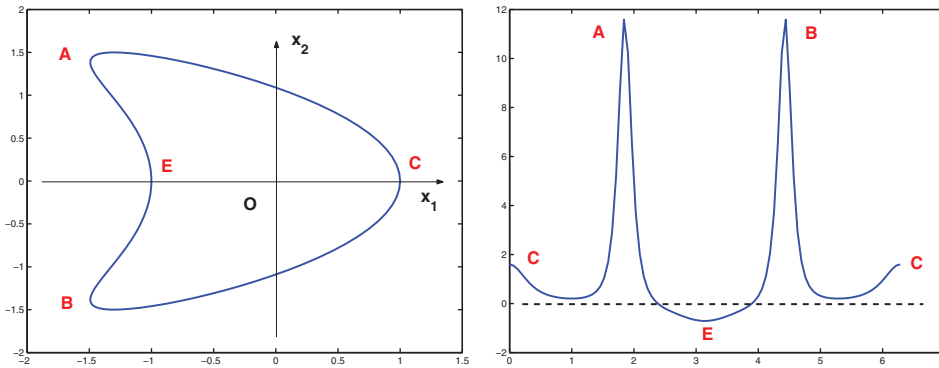


FIG. 5.6. A kite-shaped obstacle (left) and its curvature distribution with respect to the polar angle (right). The curvature takes a maximum value near points A and B, which means a strong scattering in this part.

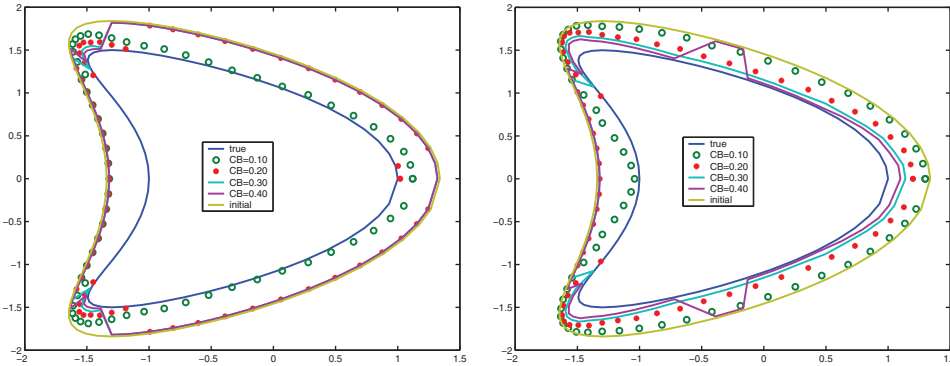


FIG. 5.7. Reconstruction for the constant surface impedance $\sigma(x) \equiv 5$ (left) and $\sigma(x) \equiv 5 - 5i$ (right). For real surface impedance, the part of the boundary with the maximum curvature is relatively easy to detect for the same blowing-up value. For $\sigma(x) \equiv 5 - 5i$ with blowup value $CB = 0.4$, the reconstruction is not improved from the initial guess for the part with minimum absolute value of curvature, due to the constant imaginary part.

Step 2. As we have explained, the nonuniform blowing-up property comes from the variation of the curvature. Now let us consider the curvature effect when the imaginary part of surface impedance is introduced. We take $\sigma(x) = 5 + \sigma^i(x)i$. The reconstructions with $\sigma^i(x)$ satisfying $\frac{1}{2}\mathcal{C}(x) + \kappa\sigma^i(x) \equiv -5$ (left) and $\frac{1}{2}\mathcal{C}(x) + \kappa\sigma^i(x) \equiv -10$ (right) in ∂D are shown in Figure 5.8.

Comparing the two pictures in Figure 5.8, it can be seen that the uniform blowing-up property is obtained, except on the parts near the point E, where the curvature takes the negative minimum value. This phenomena is physically reasonable, since the obstacle near the point E is like a basin. There are multiple reflections of the scattered wave. Due to this multiple reflection and the energy absorbing of the real part of surface impedance, the information about this concave side is relatively small in the far field data. Therefore this part cannot be improved too much. To explain more about this phenomenon, a higher asymptotic expansion using higher multipole sources is needed. This will be done in a forthcoming work.

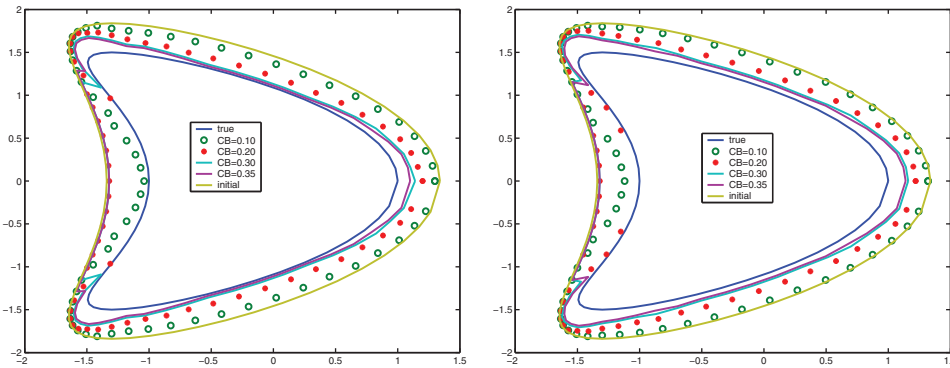


FIG. 5.8. Reconstruction for the surface impedance relating to the curvature: $\frac{1}{2}\mathcal{C}(x) + \kappa\sigma^i(x) \equiv -5$ (left) and $\frac{1}{2}\mathcal{C}(x) + \kappa\sigma^i(x) \equiv -10$ (right). The introduction of the variable imaginary part of surface impedance in terms of the curvature distribution removes the nonuniform blowing-up phenomena due to the curvature distribution.

Acknowledgment. The first author thanks the Johann Radon Institute for Computational and Applied Mathematics for its support and hospitality during his stay there.

REFERENCES

- [1] H. AMMARI, E. IAKOVLEVA, D. LESSELIER, AND G. PERRUSSON, *MUSIC-type electromagnetic imaging of a collection of small three-dimensional inclusions*, SIAM J. Sci. Comput., 29 (2007), pp. 674–709.
- [2] J.L. BUCHANAN, R.P. GILBERT, A. WIRGIN, AND Y. XU, *Marine Acoustics: Direct and Inverse Problems*, SIAM, Philadelphia, 2004.
- [3] F. CAKONI AND D. COLTON, *Qualitative Methods in Inverse Scattering Theory*, Interaction Mech. Math., Springer, Berlin, 2006.
- [4] F. CAKONI, D. COLTON, AND P. MONK, *The determination of the surface conductivity of a partially coated dielectric*, SIAM J. Appl. Math., 65 (2005), pp. 767–789.
- [5] J. CHENG, J.J. LIU, AND G. NAKAMURA, *The numerical realization of the probe method for the inverse scattering problems from the near field data*, Inverse Problems, 21 (2005), pp. 839–855.
- [6] D. COLTON AND F. CAKONI, *The determination of the surface impedance of a partially coated obstacle from far field data*, SIAM J. Appl. Math., 64 (2004), pp. 709–723.
- [7] D. COLTON AND A. KIRSCH, *A simple method for solving inverse scattering problems in the resonance region*, Inverse Problems, 12 (1996), pp. 383–393.
- [8] D. COLTON AND R. KRESS, *Inverse Acoustic and Electromagnetic Scattering Theory*, 2nd ed., Springer, Berlin, 1998.
- [9] A.J. DEVANEY, *Super resolution processing of multi-static data using time reversal and MUSIC*, J. Acoustical Soc. Amer., to appear.
- [10] K. ERHARD AND R. POTTHAST, *A numerical study of the probe method*, SIAM J. Sci. Comput., 28 (2006), pp. 1597–1612.
- [11] N. HONDA, G. NAKAMURA, R. POTTHAST, AND M. SINI, *The no-response approach and its relation to non-iterative methods for the inverse scattering*, Ann. Mat. Pura Appl. (4), 187 (2008), pp. 7–37.
- [12] D.J. HOPPE AND Y. RAHMAT-SAMII, *Impedance Boundary Conditions in Electromagnetics*, Taylor and Francis, Washington, D.C., 1995.
- [13] M. IKEHATA, *Reconstruction of obstacles from boundary measurements*, Wave Motion, 3 (1999), pp. 205–223.
- [14] V. ISAKOV, *Inverse Problems for Partial Differential Equations*, 2nd ed., Appl. Math. Sci. 127, Springer, Berlin, 2006.
- [15] A. KIRSCH, *Characterization of the shape of a scattering obstacle using the spectral data of the far field operator*, Inverse Problems, 14 (1998), pp. 1489–1512.

- [16] R. KRESS, *Linear Integral Equations*, Springer, Berlin, 1989.
- [17] J.J. LIU AND M. SINI, *How to Make the Reconstruction of Obstacles More (or Less) Accurate from Exterior Measurements*, RICAM Preprint 2008-04, Johann Radon Institute for Computational and Applied Mathematics, Linz, Austria, 2008.
- [18] J.J. LIU, G. NAKAMURA, AND M. SINI, *Reconstruction of the shape and surface impedance from acoustic scattering data for an arbitrary cylinder*, SIAM J. Appl. Math., 67 (2007), pp. 1124–1146.
- [19] G. NAKAMURA AND M. SINI, *Obstacle and boundary determination from scattering data*, SIAM J. Math. Anal., 39 (2007), pp. 819–837.
- [20] G. NAKAMURA, R. POTTHAST, AND M. SINI, *Unification of the probe and singular sources methods for the inverse boundary value problem by the non-response test*, Comm. Partial Differential Equations, 31 (2006), pp. 1505–1528.
- [21] R. POTTHAST, *Point Sources and Multipoles in Inverse Scattering Theory*, Res. Notes Math. 427, Chapman and Hall/CRC, Boca Raton, FL, 2001.
- [22] R. POTTHAST, *Sampling and probe methods - an algorithmical view*, Computing, 75 (2005), pp. 215–235.
- [23] R. POTTHAST, *A survey on sampling and probe methods for inverse problems*, Inverse Problems, 22 (2006), pp. R1–R47.
- [24] A. RAMM, *Wave Scattering by Small Bodies of Arbitrary Shapes*, World Scientific, Singapore, 2005.